Supporting information

Highly Tough All-Solid-State Ionic Conductors Based on Supramolecular Deep Eutectic Polymers for Stretchable Wearable Sensors

*Deng Qi‡, Chen Geng‡, Chen Yongsong, Zhao Hanyu, Mo Xinyu, Zhao Jiali, Wang Xiaochun, and He Minghui *, and Chang Hefeng **

Deng Qi, Chen Yongsong, Zhao Hanyu, Mo Xinyu, Zhao Jiali, Wang Xiaochun, and He Minghui

State Key Laboratory of Advanced Papermaking and Paper-based Materials, School of Light Industry and Engineering, South China University of Technology, Guangzhou 510640, China.

E-mail: heminghui@scut.edu.cn

Chen Geng and Chang Hefeng

China Banknote Security Printing Technology Research Institute Co. Ltd, Beijing 100070, China.

E-mail: chhefeng@outlook.com

‡These authors contributed equally to this work.

* Corresponding author

Experimental Section

Materials.

Betaine monohydrate (Btm, 99%, Shanghai Macklin Biochemical Technology Co., Ltd.), Acrylic acid (AA, >99%, Shanghai Macklin Biochemical Technology Co., Ltd.), Hydroxyethyl cellulose (HEC, 2% viscosity: 25-150 mpa.s, 25°C, Shanghai Macklin Biochemical Technology Co., Ltd.), Diphenyl(2,4,6-trimethylbenzoyl)phosphine oxide (photoinitiator TPO, ≥98%, Tianjin Jiuri New Materials Co., Ltd.), N-hexane (97%, Shanghai Macklin Biochemical Technology Co., Ltd.), Tetrahydrofuran (99%, Shanghai Macklin Biochemical Technology Co., Ltd.) , Ethanol anhydrous (>99%, Shanghai Macklin Biochemical Technology Co., Ltd.), 184 silicone elastomer (Dow Corning SYLGARD), and electroluminescent ZnS:Cu powders (Shanghai KPT company), were used as received.

Preparation of HEC-PDES Mixtures and ARCDEPs.

First, 0–5 wt.% HEC powder was mixed with 4.3236 g of AA and 4.0548 g of Btm. The mixture was then stirred uniformly at 60 °C for 1 h to obtain a transparent and homogeneous solution. Subsequently, 0.0216 g of photoinitiator TPO (0.5 wt.% relative to the mass of AA) was added to the above solution, followed by stirring at 60 °C for an additional 10 min to obtain PDES mixtures with varying HEC contents. The HEC-PDES mixture was then poured into a silicone model (1 mm thick) sandwiched between two glass plates and subjected to photopolymerization under UV light (20 $mW.cm^{-2}$) at room temperature for 10 min. The resulting elastomers were designated as ARCDEPs-x, where x represents the weight percentage of HEC relative to the mass of monomer AA.

Fabrication of Strain Sensors.

ARCDEPs samples were prepared using rectangular silicone molds with dimensions of 30 mm × 10 mm × 1 mm and 30 mm × 10 mm × 0.1 mm. The resistance changes induced

by strain were monitored in real time by connecting the samples to a Keithley DMM2450 digital source meter via copper wires. The relative resistance change rate (R_r) was calculated using the following equation: $R_r = (\Delta R/R_o) \times 100\%$ where ΔR is the change in resistance and R_o represents the initial resistance in the unstrained state. The sensitivity factor GF is calculated as follows: $GF=(\Delta R/R_o)/\varepsilon$ where ε is the strain. In the solvent sensitivity experiments, a 1 ml syringe was employed. The plunger speed was controlled to ensure that the mass of each single droplet dispensed was maintained at approximately 0.006 g.

Characterizations.

Fourier transform infrared (FTIR) spectra were recorded on a Bruker Vertex 33 spectrometer. Proton nuclear magnetic resonance (^{1}H NMR) spectra were acquired using a Bruker AVANCE III HD 400 MHz spectrometer with dimethyl sulfoxide-d6 (DMSO-d6) as the external reference. The glass transition temperatures (T_g) were determined by differential scanning calorimetry (DSC) using a 214 Polymer-NETZSCH instrument. Samples (5-10 mg) were loaded into aluminum pans and heated from -150°C to 80°C at a rate of 10°C/min under a N_2 atmosphere. The crystal structure of ARCDEPs was analyzed by X-ray diffraction (XRD) using an X'pert Powder diffractometer. Measurements were performed in the 2θ range of 10-60° with a scanning rate of 12°/min and a step size of 0.013°, using samples of 1 mm thickness. The thermal stability of ARCDEPs was evaluated by thermogravimetric analysis (TG) on a NETZSCH 209 F3 instrument. Samples (5-10 mg) were placed in ceramic pans and heated from 40°C to 800°C at 10°C/min under N_2 flow. X-ray photoelectron spectroscopy (XPS) was conducted on the Thermo Scientific K-Alpha spectrometer. Atomic force microscopy (AFM) phase images were obtained using a Bruker Dimension Icon microscope in tapping mode, with samples (10 mm diameter × 1 mm thickness) mounted on glass slides. UV-vis transmittance spectra were recorded from 400 to 800 nm using an Agilent Cary 60 spectrophotometer. Electrochemical impedance

spectroscopy (EIS) measurements were performed using a CHI660E electrochemical workstation over a frequency range of 10^6 to 10^{-1} Hz. The ionic conductivity (σ) was calculated using the equation σ = L/(R×A), where L, R, and A represent the thickness of ARCDEPs, its electrical resistance, and the contact area between ARCDEPs and surface area, respectively.

Mechanical Characterization.

The mechanical properties of the samples were evaluated using a universal testing machine (INSTRON 5565). Specimens with dimensions of 50 mm × 10 mm × 1 mm were tested at a constant tensile rate of 10 mm/min. The Young's modulus was determined from the slope of the initial linear region (0-10% strain) of the stress-strain curve, while the toughness was calculated as the area under the stress-strain curve. The rheology behavior of ARCDEPs was performed using an MCR 302e rheometer with a frequency range of 1–100 Hz at a constant shear strain of 1%. For fracture energy and crack-resistant strain characterization, pure shear tests were conducted at a tensile rate of 10 mm/min. The rectangular specimens (50 mm × 10 mm × 1 mm) were prepared in pairs - one unnotched and one notched. The notched specimens were fabricated by introducing a 20 mm linear notch from the edge to the center along the length direction. The fracture energy (Γ) was calculated using the equation: Γ=H ω(λc), where H represents the initial gauge length between clamps, and $\omega(\lambda_c)$ denotes the area under the stress-strain curve from initial loading to the critical strain.

Simulation Details (DFT).

All calculations in this work were performed using Gaussian 16 software. DFT calculations employed the B3LYP functional along with D3BJ dispersion correction. For geometry optimization and frequency calculations, the 6-311+G(d) basis set was used for all atoms. The structures of the single point energy were performed at the level of def2-

TZVPPD. The implicit solvent model (SMD) was used to account for the solvent effect, using water as the model solvent. Reduced density gradient (RDG) analysis and visualization were conducted using Multiwfn 3.8(dev) and VMD.

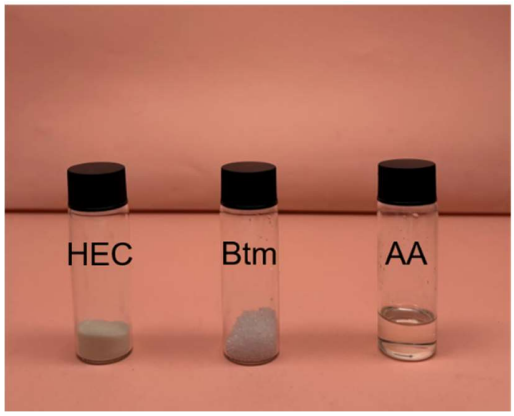

Figure S1. Digital photographs of HEC, Btm, and AA.

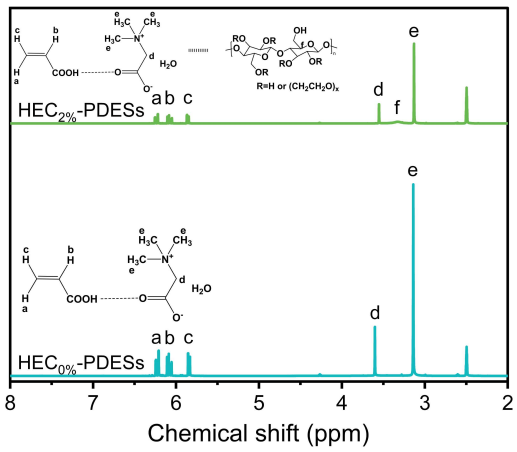

Figure S2. ^{1}H NMR spectrum of $HEC_{2\%}$-PDESs and $HEC_{0\%}$-PDESs.

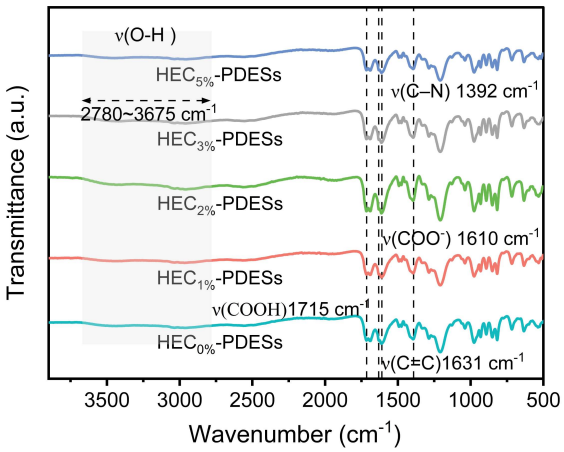

Figure S3. FTIR spectra of HEC-PDESs.

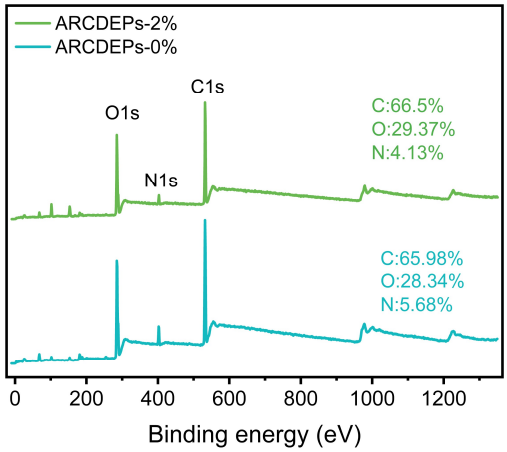

Figure S4. Full XPS spectra of ARCDEPs-2% and ARCDEPs-0%.

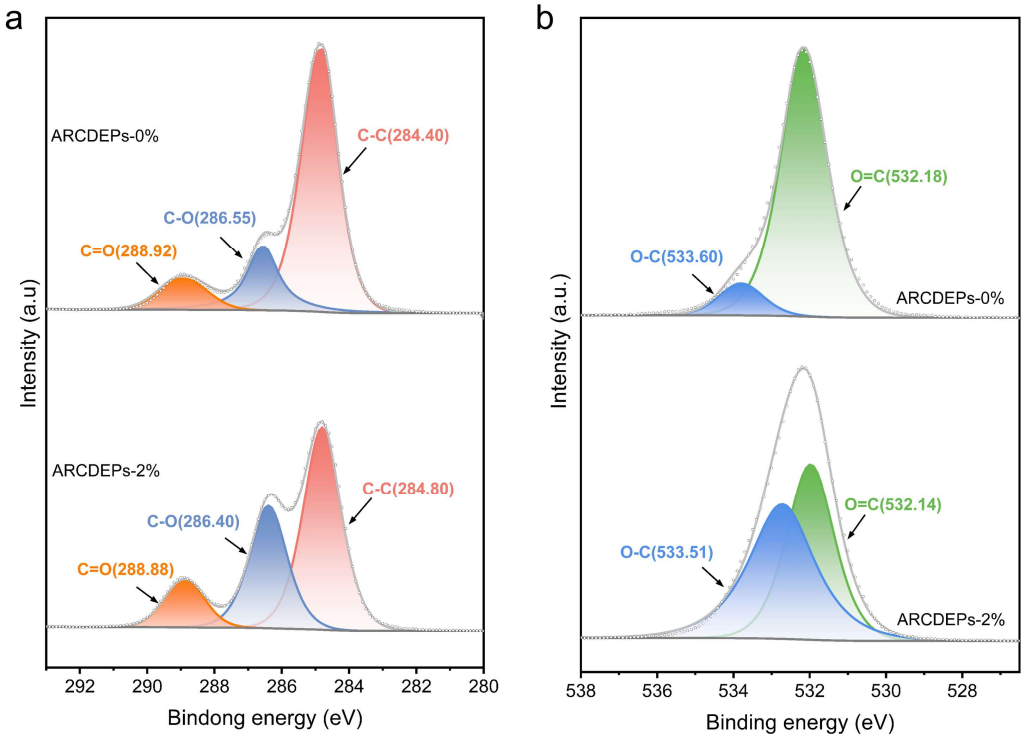

Figure S5. XPS spectra of ARCDEPs for (a) deconvoluted C 1s and (b) deconvoluted O 1s.

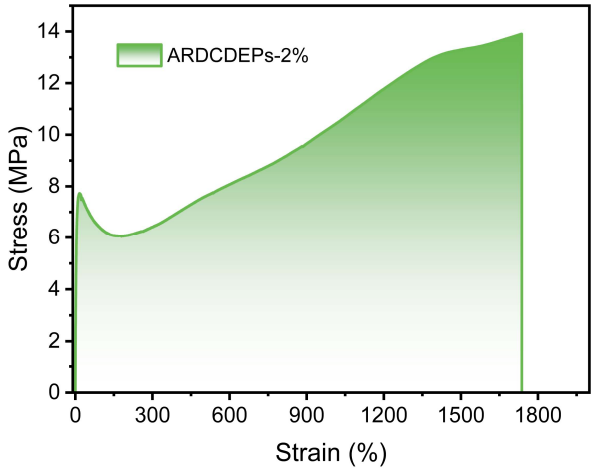

Figure S6. The toughness of the ARCDEPs-2%.

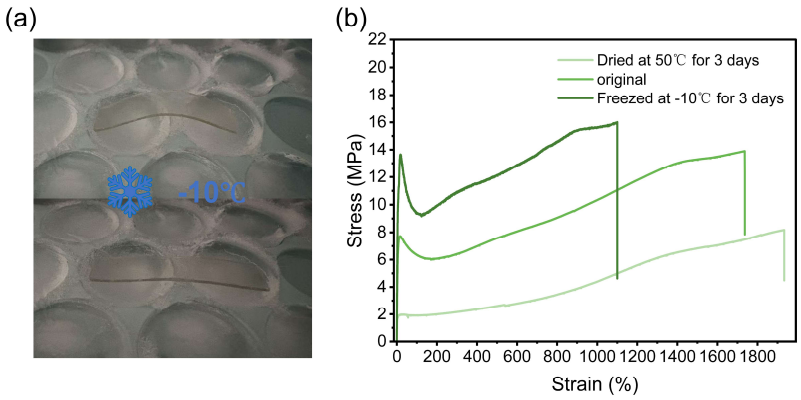

Figure S7. (a) Bending and then recovery images of ARCDEPs-2% after storage at −10℃ for 3 days; (b) stress-strain curves of ARCDEPs-2% at different temperatures.

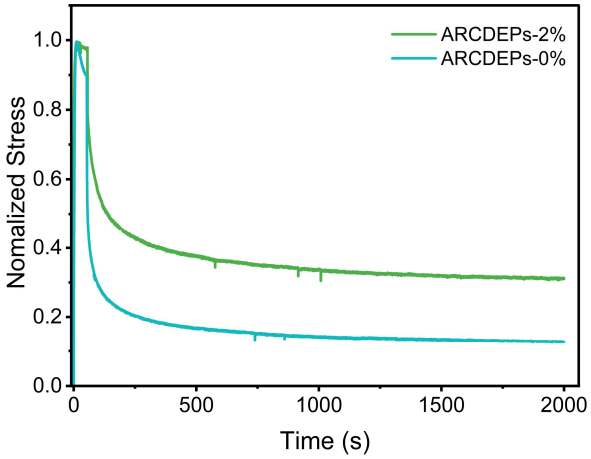

Figure S8. Stress−relaxation curves of ARCDEPs-2% and ARCDEPs-0%.

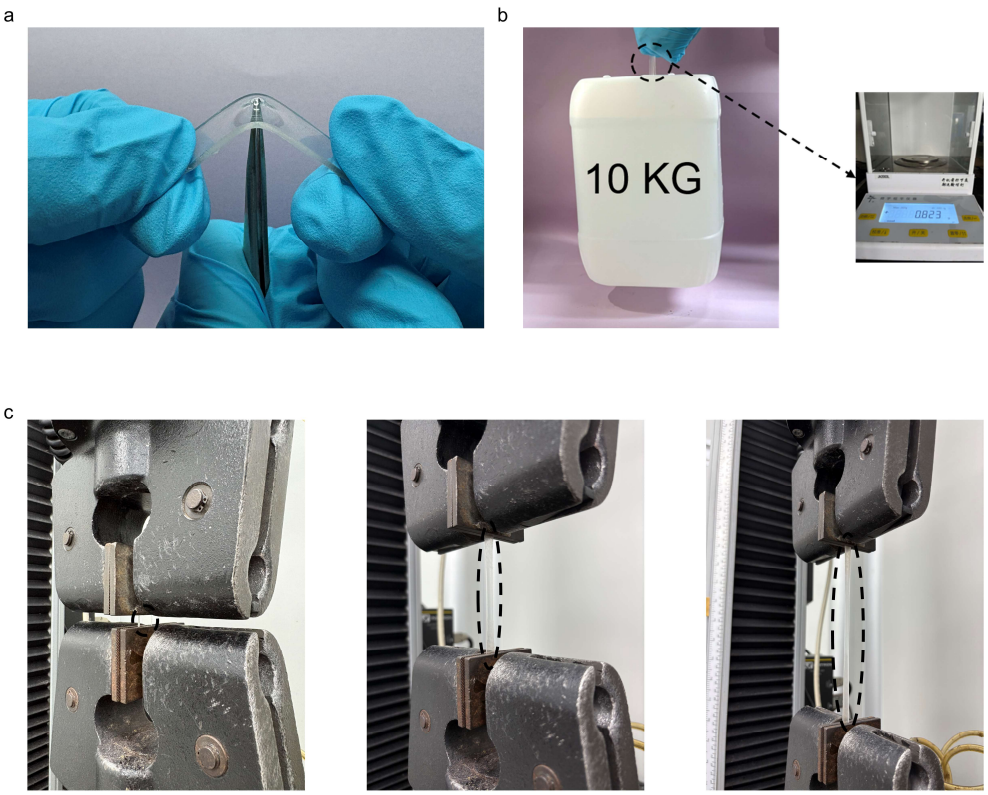

Figure S9. The puncture resistance, Stretchable changes and load-bearing test diagrams of ARCDEPs-2%.

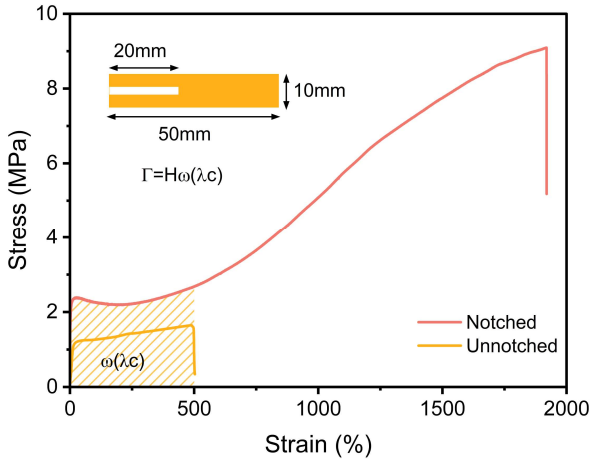

Figure S10 Stress-strain curves of without crack and with crack samples of ARCDEPs-1%.

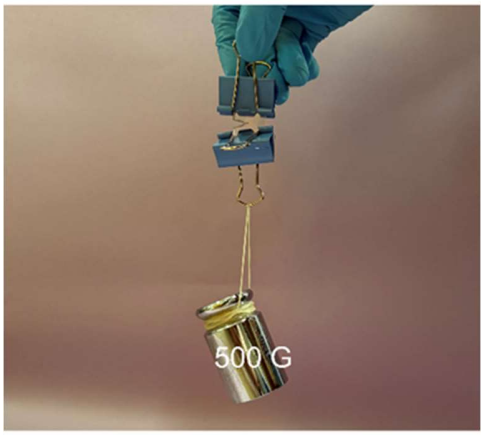

Figure S11. The crack-resistant experimental image of ARCDEPs-2%.

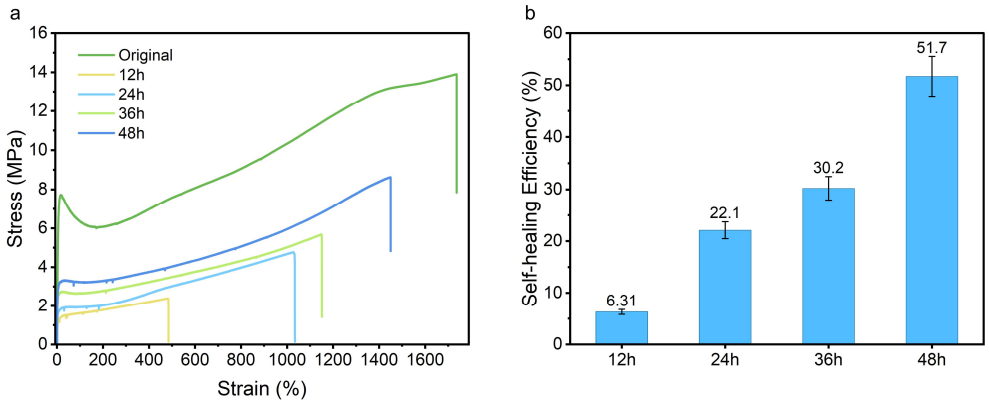

Figure S12. Self-healing properties of ARCDEPs-2%. (a) Stress–strain curves for ARCDEPs-2% mechanical self-healing. (b) Mechanical self-healing efficiency of ARCDEPs-2% at different healing times.

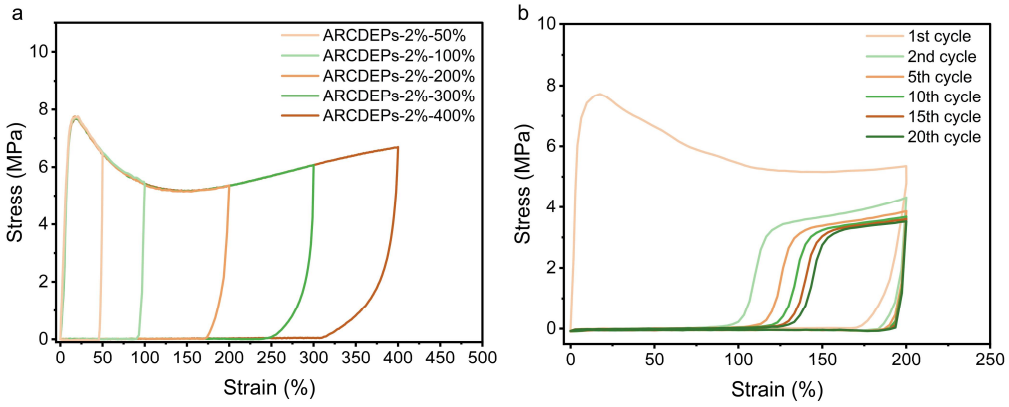

Figure S13. (a) Cyclic loading-unloading tensile tests of ARCDEPs-2% at different strains (50%, 100%, 200%,300%, 400%). (b) Cyclic loading-unloading tensile tests of ARCDEPs-

2% to 20 consecutive cycles at the 200% strain.

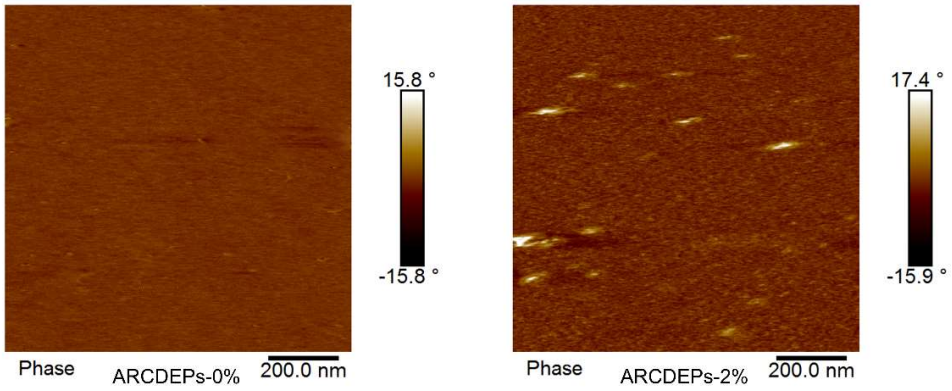

Figure S14. AFM images of the prepared ARCDEPs.

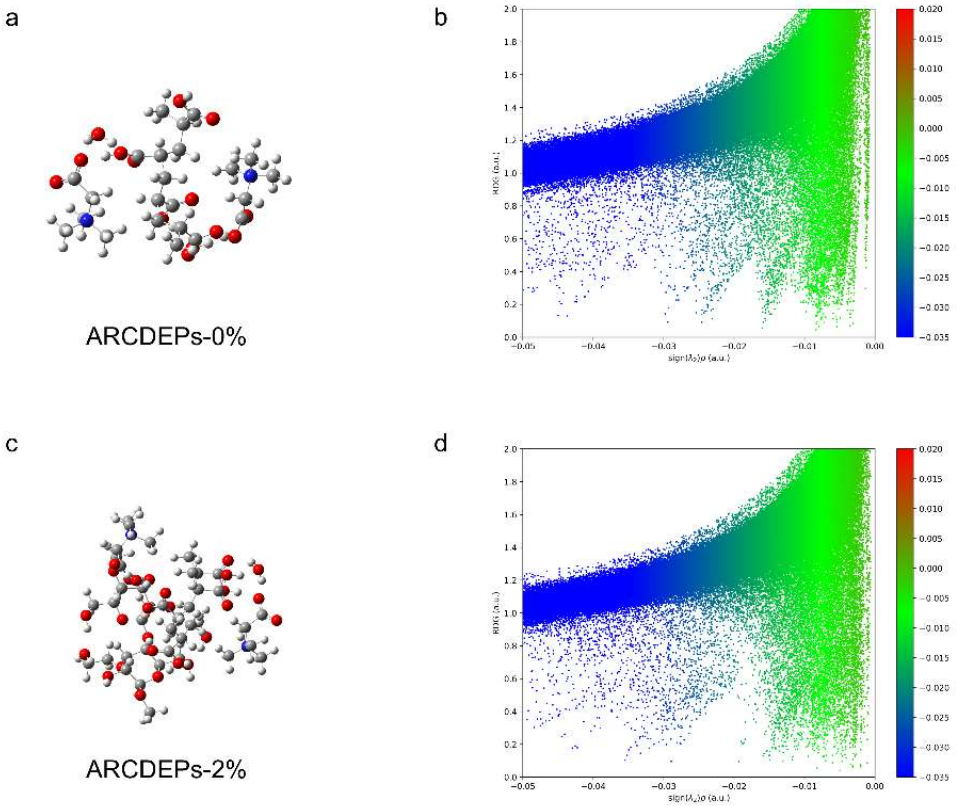

Figure S15. Density functional theory (DFT) simulation of the tow systems. (a), (c) are the optimized structures of PAA-BTM, and PAA-Btm-HEC. (b), and (d) are th e relation

diagrams of RDG and sign (λ2) ρ of PAA-BTM, and PAA-Btm-HEC, r espectively, where the sign (λ2) ρ ranges from −0.05 to 0.00.

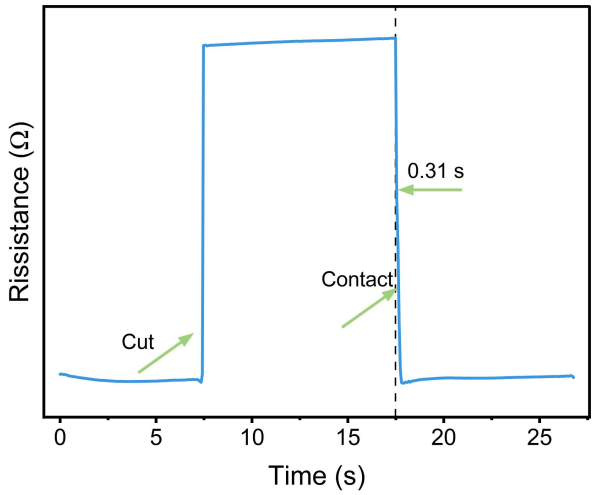

Figure S16. Resistance recovery time of ARCDEPs-2% after splicing a broken ARCDEPs-2%.

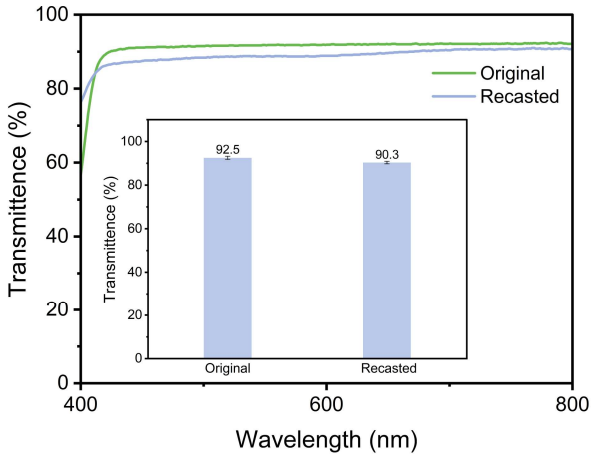

Figure S17. Optical transparency of recasted ARCDEPs-2% with a thickness of 1 mm.

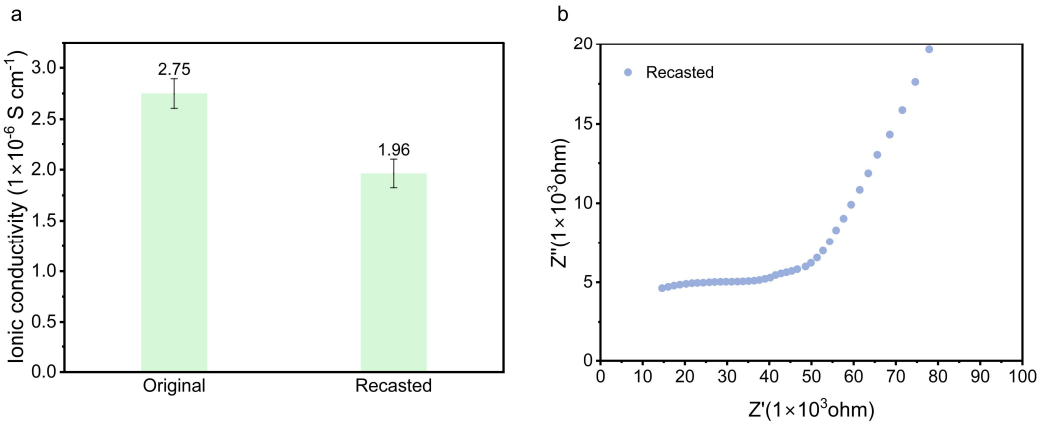

Figure S18. (a) Ionic conductivity of recasted ARCDEPs-2%. (b) Electrochemical impedance (EIS) spectra of recasted ARCDEPs-2%.

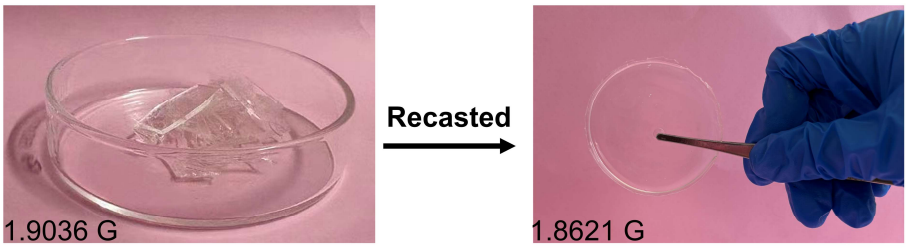

Figure S19. The mass of the ARCDEPs-2% before and after the reprocess.

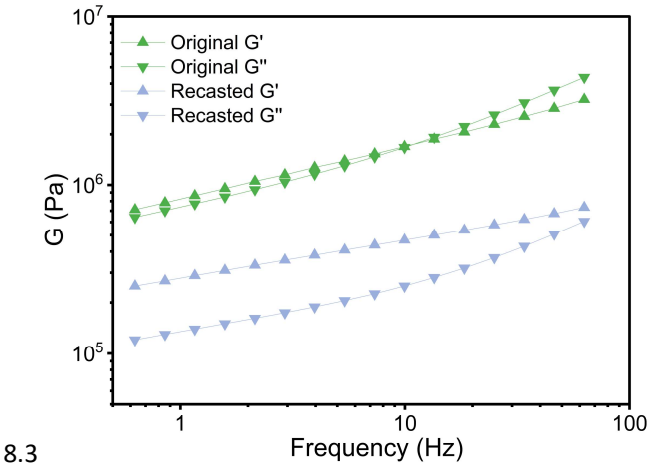

Figure S20. Storage modulus (G') and loss modulus (G'') of ARCDEPs-2% before and after recasting.

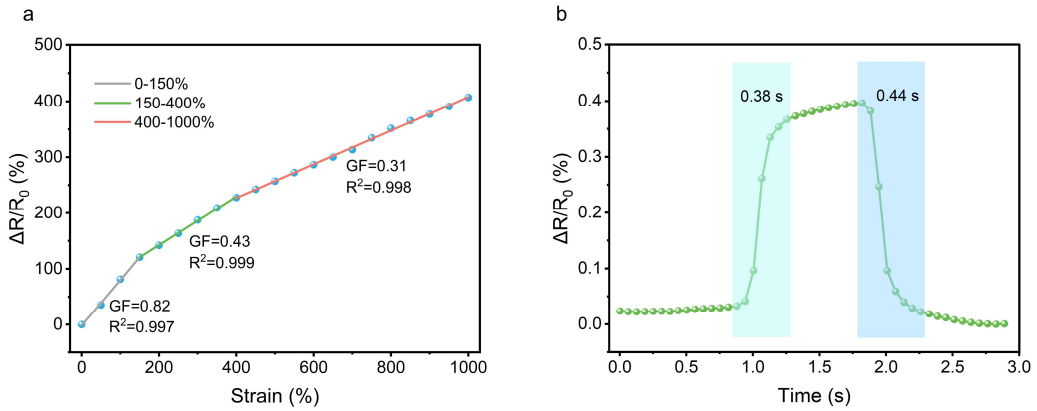

Figure S21. (a) Resistance–strain dependence of ARCDEPs-2%; gauge factors (GFs) were obtained by fitting the curve with three segments (0–150, 150-400 and 400–1000% strain). (b) Response time of ARCDEPs-2% under 1 % strain sensing.

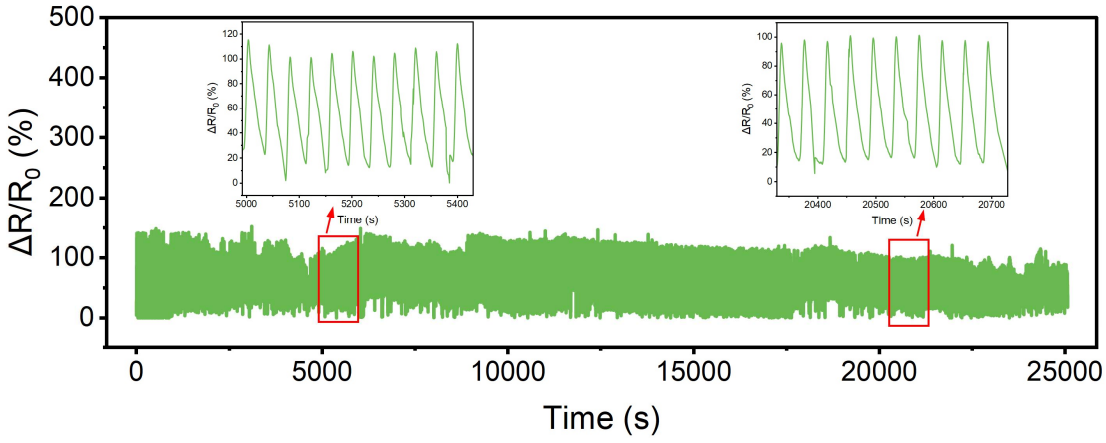

Figure S22. 1000 electrical stability tests of ARCDEPs-2% at 200% strain.

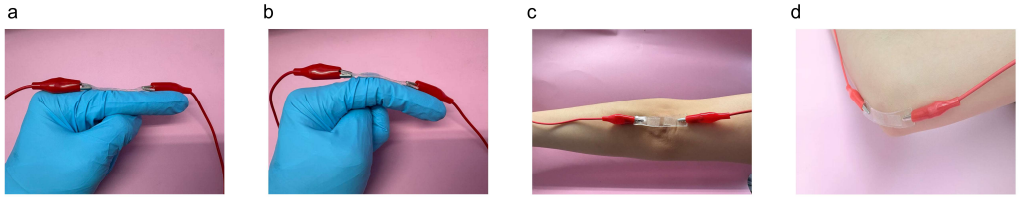

Figure S23. (a, b) Optical images of the ARCDEPs-based sensor attached on the finger by double-sided tape and bent 60°, (c, d) The ARCDEPs-based sensor is attached on the arm

by means of double-sided adhesive tape and bent 90° for optical images.

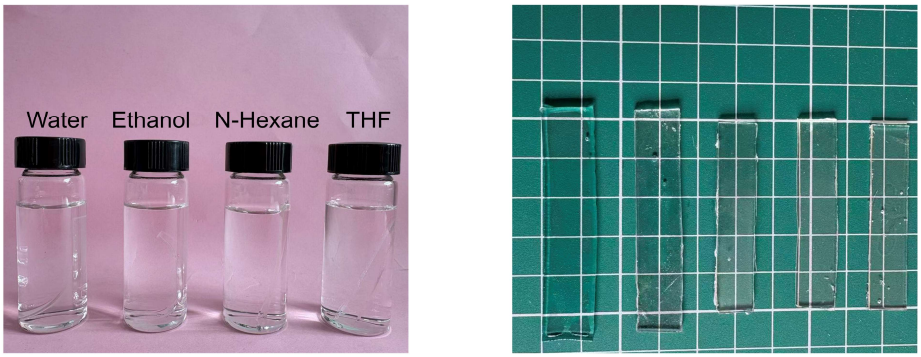

Figure S24. The swelling behavior of ARCDEPs-2% in Water, Ethanol, N-Hexane, and Tetrahydrofuran (from left to right).

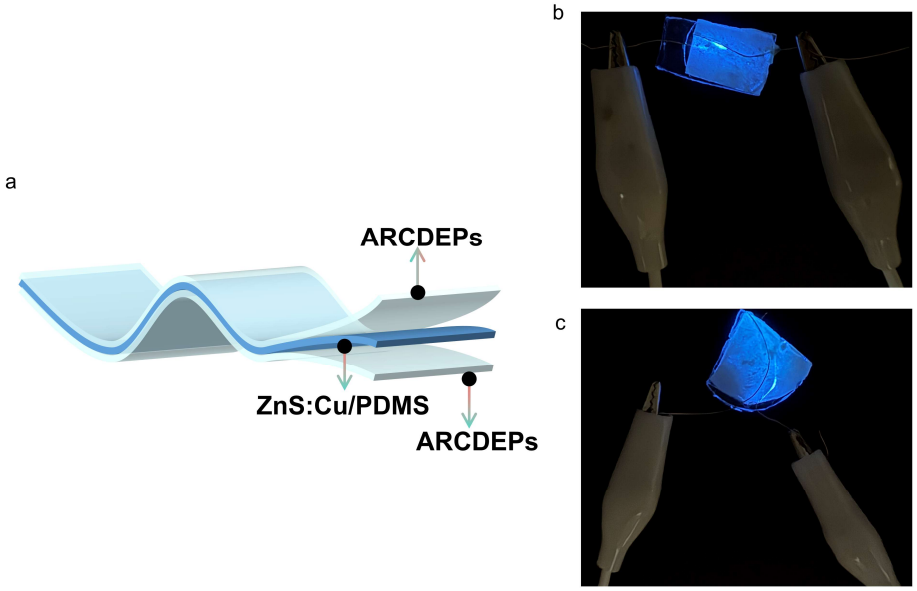

Figure S25 (a) Schematic illustration of ARCDEPs-based flexible electroluminescent devices; photographs of the flexible ARCDEPs-2%-based electroluminescent devices with (b) rectangle and (c) sector.